

Management of Low- and High-Frequency Power Components in Demand-Generation Fluctuations of a DFIG-Based Wind-Dominated RAPS System Using Hybrid Energy Storage

Mr. J. SRINU NAICK¹, Mr. AREPALLI NARASIMHA MURTHY²,

Associate Professor, Department of Electrical and Electronics Engineering#1.

M.Tech Student Department of Electrical and Electronics Engineering#2.

Abstract

This paper presents a control strategy for managing the demand-generation fluctuations using a hybrid energy storage system in a wind-dominated remote area power supply (RAPS) system consisting of a doubly fed induction generator (DFIG), a battery storage system, a super capacitor, a dump load, and main loads. Operation of a battery storage system is coordinated with a super capacitor with a view to improving the performance of the battery. In this regard, the battery storage system is connected to the load side of the RAPS system, whereas the super capacitor is connected to the dc bus of the back to back converter of the DFIG. The operation of the hybrid energy storage system is coordinated through the implementation of a power management algorithm, which is developed with a view to reducing the depth of discharge and ripple content of the battery current. In addition, the dump load is connected to the load side of the RAPS system, which utilizes the power in situations that cannot be handled via an energy storage system. In addition, a coordination method has been developed and proposed to coordinate the power flows among all system components with a view to regulating the power flow and thereby ensuring the robust voltage and frequency control on the load side while capturing the maximum power from wind.

I. INTRODUCTION

DUE TO THE variable nature of wind (i.e., intermittency), a standalone wind turbine generator alone cannot match the generated power with load demand. In this regard, for a standalone wind farm to be dispatchable similar to other conventional generation units (e.g., diesel generators), the

generated power has to be regulated at a desired level. With rapid developments currently taking

place on energy storage devices, their application in wind energy systems is seen to provide a promising opportunity to mitigate the issues associated with wind power fluctuations [1]. An energy storage system can be categorized in terms of its role in a remote area power supply (RAPS) system, i.e., either for energy management or for power quality enhancement [2].

An ideal energy storage in a standalone wind energy conversion system should be able to provide both high energy and power capacities to handle situations such as wind gusts and load step changes, which may exist for seconds or minutes or even longer. At present, various types of storage technologies are available to fulfill either power or energy requirements of a RAPS system. Widely advocated energy storage technologies that currently employ in wind farms are batteries, super capacitors, flywheels, compressed-air energy storage, hydro pumped storage, superconducting magnetic energy storage, fuel cells, etc. [3], [4]. Energy storage systems with high energy density levels are usually termed as “long-term storage” as they are able to operate over a long period of time (e.g., minutes to hours). Similarly, energy storage systems with high power density are termed as “short-term storage” as they are capable of handling transients that occur over a short period of time (e.g., seconds to minutes).

Among all energy storage systems, batteries are seen to have one of the highest energy density levels, whereas the super capacitors seem to have the highest power density. At present, battery storage systems are

widely employed in most real-life RAPS applications [5]. To further improve the performance of the battery energy storage systems, a super capacitor can be incorporated to perform a hybrid operation [6], [7]. In this way, the combined energy storage system is able to satisfy both power and energy requirements of the RAPS system.

Recent studies [8]–[10] in relation to the modeling and control aspects of an energy storage system for a grid connected wind application have received substantial attention. On the contrary, work related to standalone wind energy storage systems has received only little research attention. The applicability of batter storage as the energy storage for a grid connected variable wind generator is described in [9] and [10]. As reported in this literature, the core objective behind the use of the energy storage system (i.e., battery banks) is to mitigate the effect of wind speed fluctuations and thereby to ensure smooth power

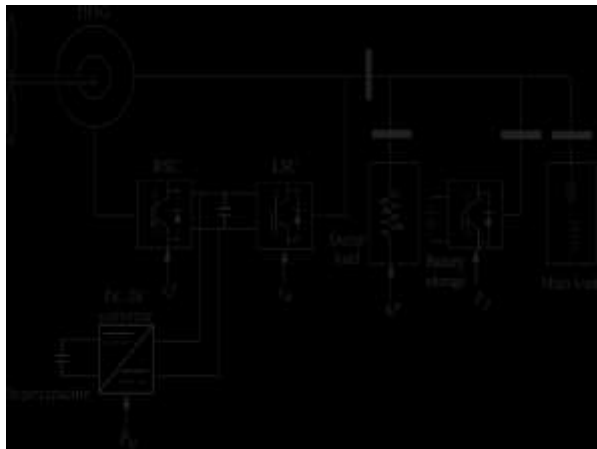


Fig.1. Hybrid energy storage in a DFIG-based RAPS system.

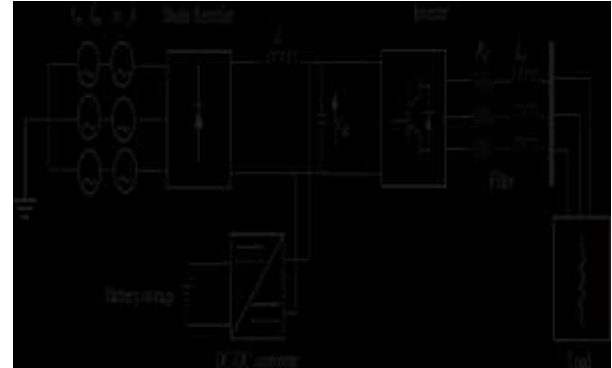


Fig.2. Schematic of the simplified standalone power supply system.

output from the wind turbine generator. A hybrid energy storage system, including both battery system and super capacitor, for a grid connected variable wind turbine generator is discussed in [6]. The application of a hybrid energy storage system for grid connected and standalone wind energy applications is given in [6] and [11], respectively. This literature particularly focuses on the performance of the hybrid energy storage system rather than considering the system-level investigations.

The RAPS system considered in this paper is shown in Fig. 1 consisting of a wind turbine generator; a hybrid energy storage system, namely, battery energy storage and super capacitor; a dump load; and main loads. In this regard, individual controllers for the system components have been developed, and their operations are coordinated with a view to regulating the load-side voltage and frequency and to extracting maximum power from wind. In addition, a power management algorithm is implemented between two energy storage devices (i.e., battery storage and super capacitor) with a view to ensuring safer operation of the battery storage system by avoiding higher depth of discharges (DODs). The suitability of the propped RAPS system is investigated under changing wind and fluctuating load conditions.

This paper is organized as follows. Section II illustrates the importance of having integrated an energy storage system for renewable energy (i.e.,

wind) application. The significance of hybrid energy storage for a wind energy application is also illustrated in this section. Section III discusses the proposed control coordination methodology employed among the components in the RAPS system. The detailed information of the proposed power management algorithm adopted to the battery energy storage system and super capacitor is described in Section IV. The individual control strategies developed for each RAPS system component [e.g., doubly fed induction generator (DFIG) and battery energy storage] are given in Section V. The simulated results of the proposed RAPS system are presented in Section VI. Conclusions are given in Section VII.

II. BENEFITS OF INTEGRATING ENERGY STORAGE FOR RAPS SYSTEM

Two examinations that are based on two different circuits shown in Figs. 2 and 6 are used to illustrate the benefits of having integrated: 1) battery energy storage; and 2) hybrid energy storage for wind energy application, respectively.

The arrangement shown in Fig. 2 can be used to investigate the benefits of having energy storage for a standalone wind system. To represent the intermittency associated with the wind turbine power output, a variable power supply that consists of a steady component v_m of 230 V at a fundamental frequency f_m of 50 Hz and a variable supply at a frequency f_s of 120 Hz with a voltage source of magnitude v_s of 50 V is used.



Fig.3. Controller for the energy storage system.

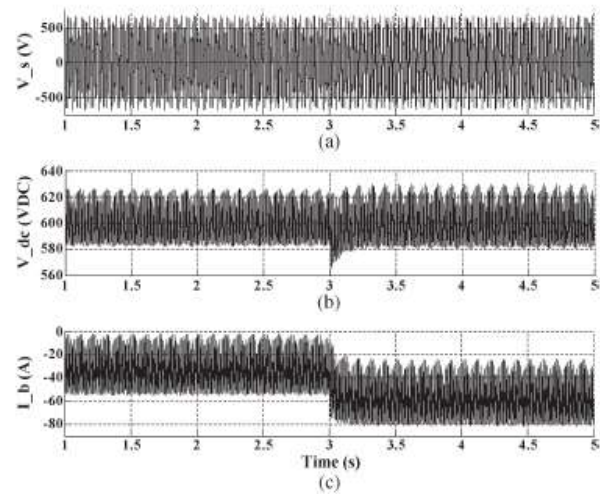


Fig. 4. RAPS system performance with the battery storage system: (a) supply voltage, (b) dc link voltage, and (c) battery current.

As shown in Fig. 2, a battery system is selected to represent the energy storage system, which is incorporated into the dc bus of the wind energy system. The main objective of the battery storage system is to regulate dc bus voltage v_{dc} . In this regard, a bidirectional boost converter is used to interface the battery storage system to the dc bus. The conditions under which the battery storage system is operated can be explained by (1). Any power imbalance associated with the RAPS system shown in Fig. 2 can lead to a dc bus voltage variation. Hence, the dc bus voltage variation is used as the input signal of the controller, as shown in Fig. 3, for the battery storage system

$$\text{battery status} = \begin{cases} \text{charging mode,} & \Delta v_{dc} > 0 \\ \text{discharging mode,} & \Delta v_{dc} < 0 \\ \text{idling mode,} & \Delta v_{dc} = 0. \end{cases} \quad (1)$$

The suitability of the energy storage system, which helps in regulating the dc link voltage, is observed under fluctuating wind and load conditions. Initially, the load is set at 25 kW, and after $t=3$ s, the load demand is increased to 40 kW. The supply-side voltage, which is used to simulate the power output of the wind turbine generator, is shown in Fig. 4(a).

The simulated behavior of the dc bus and load-side voltage with and without the energy storage system are shown in Figs. 4(b) and 5, respectively. The corresponding battery storage current is shown in Fig. 4(c). It is shown that the dc link voltage is regulated within $\pm 5\%$ of its rated value (i.e., 600 V) in the presence of the battery storage system. In contrast, the variation of dc link voltage without the battery storage system is seen to vary within +5% and -15% of its rated value. This simulation exercise clearly indicates the benefits of the energy storage

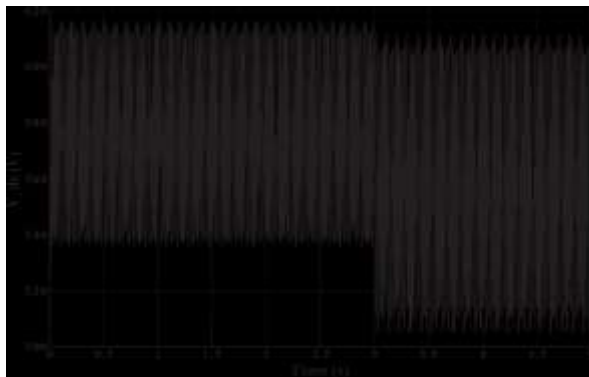


Fig. 5. DC link voltage in the absence of the battery storage.



Fig. 6. Simplified model of a power system with hybrid energy storage.

System for a standalone wind application. However, it can be noted that the current of battery energy storage is fluctuating rapidly. This may adversely affect the life span of the battery storage system. Therefore, it is vital to hybridize the operation of the battery storage system with a super capacitor that could relieve the fluctuating effects in operation of the battery storage system.

A simple arrangement² shown in Fig. 6 is used to demonstrate the significance of integrating hybrid energy storage into a standalone wind power application where the fluctuating current source represents the variable wind power output, which consists of two components. The main steady component corresponds to dc current with a magnitude of $A = 50$ A and a ripple component of $B = 7.5$ A at $f = 20$ Hz that is superimposed on the main component to simulate the fluctuating power component of the wind turbine generator. The battery storage system is represented by the series resistor r_b with a constant dc voltage source v_b of 25 V. The super capacitor is represented

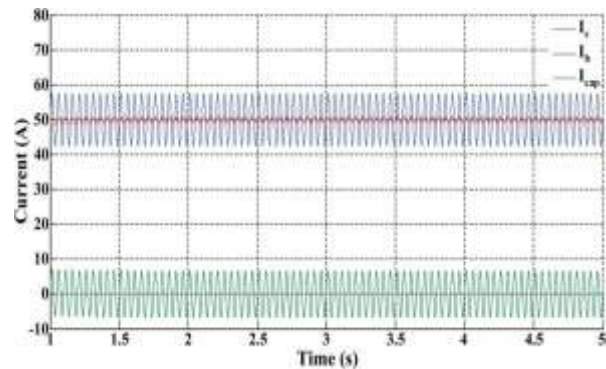


Fig. 7. Current sharing between battery storage and super capacitor.

by a capacitor of which the voltage is v_{cap} , connected in series with resistor r_{cap} .

The simulated behavior of the system is shown in Fig. 7. It is shown that the fluctuating component of the current is absorbed by the super capacitor, whereas the battery storage System absorbs the steady component of 50 A. The fluctuation of the battery current is limited to ± 1 A, thus ensuring safe operation of the battery storage system. The above example demonstrates the benefits of having integrated a super capacitor with battery energy storage for effectively mitigating the ripple content of the battery current.

III. PROPOSED COORDINATED CONTROL APPROACH FOR HYBRID

ENERGY STORAGE-BASED RAPS SYSTEM

The decision-making process associated with the control coordination algorithm of the wind–battery–super capacitor based RAPS system is shown in Fig. 8. During over generation conditions where the power output from the wind turbine generator P_w is greater than the load demand P_L , the hybrid energy storage P_b (i.e., battery storage and super capacitor) absorbs the excess power ($P_w - P_L$) and is shared between the battery storage system and super capacitor according to the power management algorithm presented in Section IV.3 If the capacity of the hybrid energy storage system reaches the maximum limit or $(P_b)_{max}$, the dump load needs to absorb the excess power. However, if the dump load power P_d reaches its maximum rating $(P_d)_{max}$, the pitch angle control has to be activated in order to reduce the power output of the wind turbine generator. During under generation situations where the power output of the wind turbine generator is less than the load demand, i.e., $(P_w - P_L) < 0$, it is assumed that the hybrid energy storage P_b is able to supply the required power deficit $(P_L - P_w)$. During emergency situations such as no power output from wind turbine generator due to wind speed being below cut-in level or above cut-out level, a load shedding scheme can be implemented, which is not given an emphasis in this paper. Moreover, the proposed control coordination concept has been realized by developing the control strategies for each component of the RAPS system.

It is assumed that the entire reactive power requirement of the RAPS system Q_L is satisfied using DFIG, i.e., QDFIG. More information regarding the reactive power generation through the DFIG is illustrated in Section V-A. However, it is to be noted that, for the case where a higher value of reactive power is required, a capacitor bank can be installed.

IV. PROPOSED POWER MANAGEMENT ALGORITHM FOR HYBRID ENERGY STORAGE SYSTEM

Depending on the objectives to be achieved (e.g., minimization of the demand-generation mismatch and ensuring safe operation of the energy storage systems), a power management algorithm can be designed and implemented for the hybrid energy storage system. The proposed power management algorithm is designed in such a way that the super capacitor should be able to absorb the ripple or high-frequency power component of demand-generation mismatch leaving the steady component for the battery storage system. As indicated in Section III, the power management algorithm is implemented encompassing the battery storage and super capacitor with a view to achieving the following objectives:

- 1) to help maintain the power balance of the RAPS system;
- 2) to operate the wind turbine generator based on the maximum power point tracking (MPPT) algorithm;
- 3) To improve the performance of the battery storage system by reducing ripple current and high rate of DOD.

The first objective is achieved by generating the input signal for the controllers of the hybrid energy storage system using the demand-generation mismatch $(P_w - P_L)$ of the RAPS system. To realize the second objective, the wind power output P_w of the demand-generation mismatch is estimated using the optimal wind power $(P_w)_{opt}$ given by (2)–(4). By controlling the power flow into/out of the battery storage system and super capacitor, it is possible to impose an appropriate torque on the wind turbine generator to extract the maximum power from wind. In this way, maximum power tracking algorithm is embedded with the power management scheme to extract the maximum available power from wind

$$(P_w)_{opt} = k_{opt} [(\omega_r)_{opt}]^3 \tag{2}$$

$$k_{opt} = \frac{1}{2} (C_p)_{opt} \rho A \left(\frac{R}{\lambda_{opt}} \right)^3 \tag{3}$$

$$\lambda_{opt} = \frac{(\omega_r)_{opt} R}{v} \tag{4}$$

where $(C_p)_{opt}$ is the optimum power coefficient of the turbine, A is the area swept by the rotor blades, v is the wind speed, ρ is the air density, R is the radius of the blade, λ_{opt} is the optimum tip-speed ratio, β is the pitch angle, and $(P_w)_{opt}$ is the optimal wind power output.

Under heavy DOD levels, the battery storage attains quick charge regulation, as shown in Fig. 9. Therefore, the third objective is related to managing the DOD levels of the battery storage system, which is achieved by separating the demand-generation mismatch into two frequency components through a high-pass filter $\tau s/1 + \tau s$, as shown in Fig. 10. The

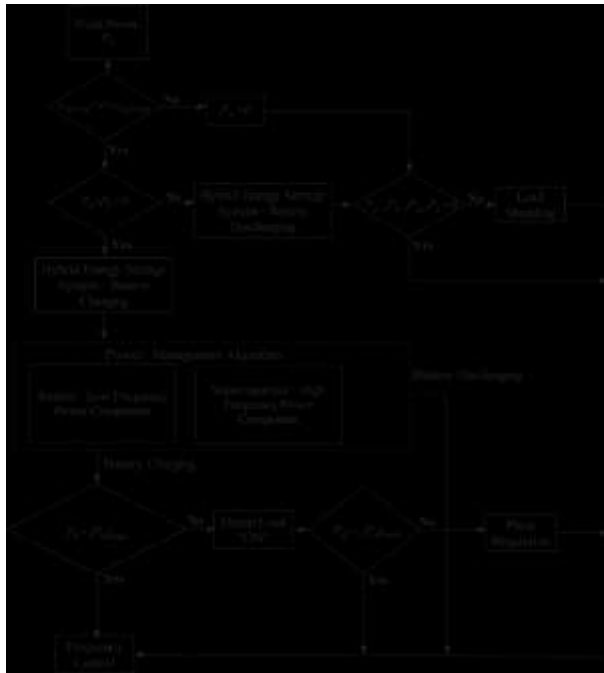


Fig.8. Control coordination of a wind–battery–super capacitor-based hybrid RAPS system

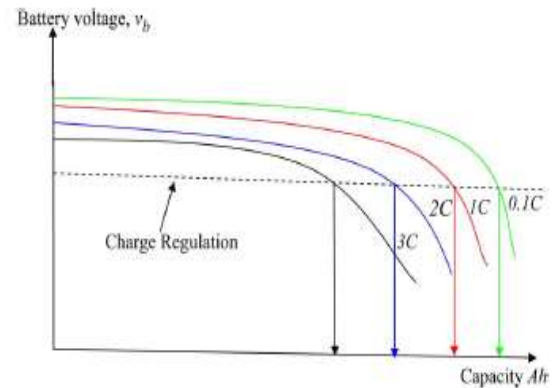


Fig. 9. Battery voltage under different discharge rates. (C denotes the discharge rate of the battery storage system.)

Demand-generation mismatch is explained by two frequency regions, which can be given by (5). The high-frequency power component of the demand-generation mismatch P_{hf} is used to estimate the reference current of the super capacitor $(i_c)_{ref}$. Contrarily, the low-frequency power component of the demand generation mismatch P_{lf} is used to generate the reference current of the battery storage $(i_b)_{ref}$. The operating frequency

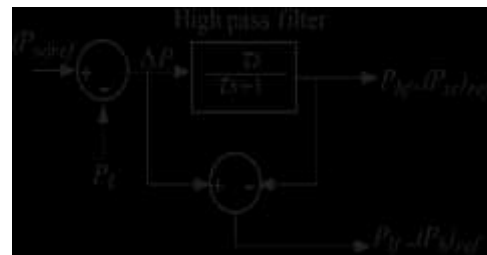


Fig. 10. Estimation of reference power for battery storage and super capacitor.

$$\Delta P_{wL} = P_{hf} + P_{lf} \quad (5)$$

Where P_{hf} is the high-frequency component of the demand generation mismatch, and P_{lf} is the low-frequency component of the demand-generation mismatch.

Considering the operating frequency range as the criterion, two different models of a super capacitor can be depicted, as

4fc represents the cutoff frequency of the filter circuit. Typically, fc is 0.5 Hz [6].



Fig. 11. Operating frequency ranges of the energy storage systems: Super capacitor and battery storage system.

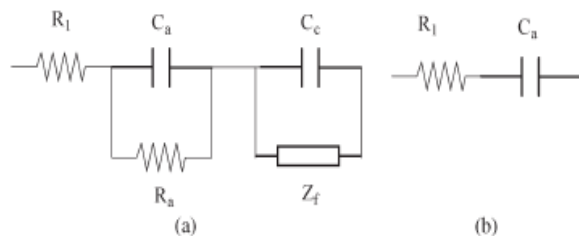
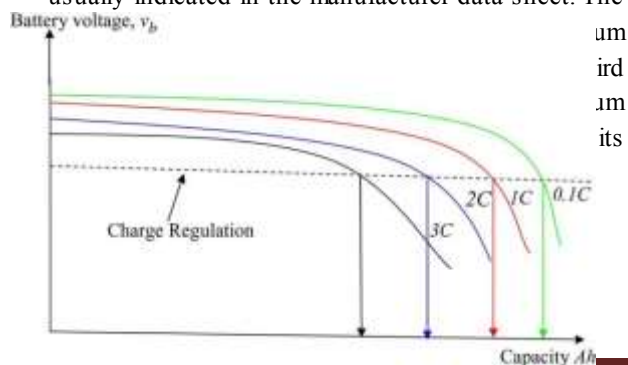


Fig. 12. Equivalent circuits of super capacitor. (a) High-frequency model. (b) Low-frequency model.

shown in Fig. 12. The first model indicated in Fig. 12(a) is known as detailed model, which includes the nonlinear Faraday capacitance. The low-frequency domain model, which can be used under power system operating frequency range presented in Fig. 12(b) is employed in the current work.

In real-life applications, the operation of a super capacitor needs to satisfy the conditions given in (6)–(8). The first condition given by (6) emphasizes the safe operating voltage of a super capacitor, which is usually indicated in the manufacturer data sheet. The



$$(v_{sc})_{\min} < v_{sc} < (v_{sc})_{\max} \quad (6)$$

$$(I_c)_{pk} = \frac{0.5C_{sup}v_{sc}}{C_{sup}(ESR_{dc}) + 1} \quad (7)$$

$$(P_{sc})_{\max} = \pm C_{sup}v_{sc} \left| \frac{dv_{sc}}{dt} \right|_{\max} \quad (8)$$

where C_{sup} is the capacitance value of the super capacitor; $(v_{sc})_{\max}$, $(v_{sc})_{\min}$ are maximum and minimum operating voltages of super capacitor, respectively; ESR_{dc} is the equivalent series resistor of the super capacitor; $(P_{sc})_{\max}$ is the maximum power rating of the capacitor, and $|dv_{sc}/dt|_{\max}$ is the maximum rate of change of voltage across the super capacitor.

The size estimation of the battery energy storage and super capacitor is extremely design specific for a given site or an application. However, in the present case, the value of the capacitance of the super capacitor is estimated considering the worst case scenario where it is able to supply energy subjected to the wind energy inverter constraints over a certain time period t , as given by (9) and (10). Furthermore, the size of the battery storage system is estimated using the condition given in (11) as follows:

$$E_{sc} = (s_{\max}(P_{DFIG})_{rated}) t \quad (9)$$

$$C_{sup} = \frac{2E_{sc}}{((v_{sc})_{\max})^2 - ((v_{sc})_{\min})^2} \quad (10)$$

$$\mu \times i_{rated} \times \left(\frac{t}{60} \right) = (Ah \text{ rating}) \times k' \quad (11)$$

Where μ is the fraction of the rated current of the load demand, i_{rated} is the rated current corresponding to the load demand, t is the time duration over which the battery provides power to the system, and k' is a fraction that defines the average discharge/charge current of the battery storage.

V. DESIGN OF CONTROLLERS FOR INDIVIDUAL SYSTEM COMPONENTS

As shown in Fig. 1, the battery storage is connected to the load side using an inverter, whereas the super capacitor is interfaced to the dc bus of the back-to-back converter system by means of a bidirectional buck boost converter. The operation of the entire RAPS system is designed according to the proposed coordinated control approach given in Fig. 8. The control strategies associated with the battery storage system, super capacitor, and dump load are illustrated in the following sections.

A. DFIG Control

The rotor-side converter (RSC) and line-side converter (LSC) are modeled as current-controlled voltage source inverters in which the field-oriented vector control schemes are employed to develop the respective control schemes. The control objectives that are related to RSC and LSC can be listed as follows:

1) RSC: voltage and frequency control on the stator side;

2) LSC: dc bus voltage control of the back-to-back converter system and it provides reactive power if necessary for loads.

The voltage controller of the DFIG is developed using a reactive-power-based control approach. In this regard, the total stator reactive power output Q_s of the DFIG can be given as

$$Q_s = \frac{3}{2} \left[-\frac{v_s^2}{\omega L_s} + v_s \frac{L_m}{L_s} i_{dr} \right]. \quad (12)$$

The rotor d-axis current i_{dr} consists of two components, i.e., magnetizing current i_{drmag} , which is used to compensate the no-load reactive power of the DFIG, and i_{drgen} , which is utilized to satisfy the reactive power requirements of the loads. The corresponding reactive power components of these two currents, namely, Q_{mag} and Q_{gen} , are given by (13) and (14), respectively,

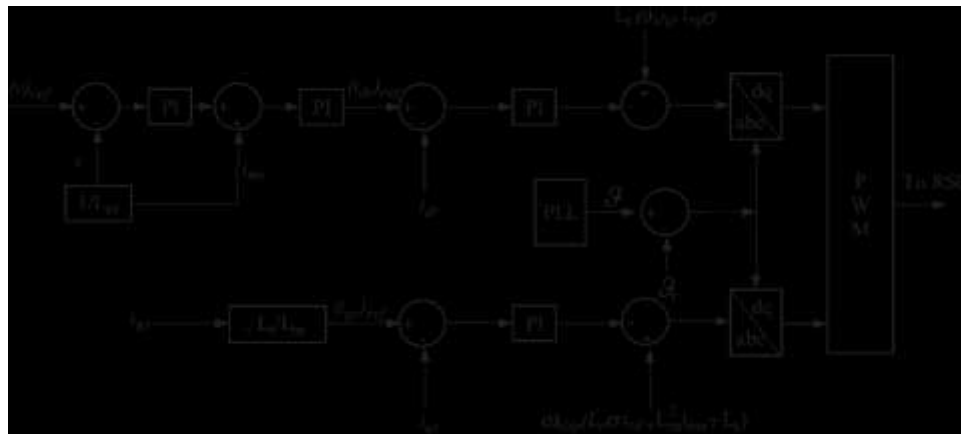


Fig.13. RSC control scheme of DFIG.

reference current of the battery (i_b)_{ref} is generated considering the low-frequency

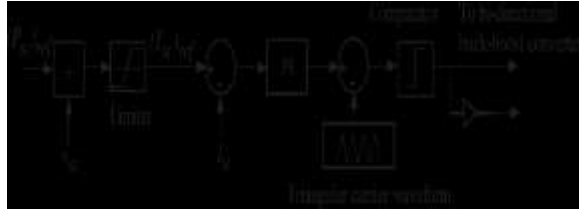


Fig. 15. Control strategy for the super capacitor in hybrid energy storage.

Component of the demand-generation mismatch P_{df} as given in (19). The inverter is operated at unity power factor by setting $(i_{qs})_{ref}$ equal to zero. The PI controllers associated with control schemes shown in Fig. 14 are tuned using the Ziegler–Nichols method, as given in [15]

$$(i_b)_{ref} = (P_{df} - P_b)(k_p + k_i/s) \quad (19)$$

Where P_b is the actual battery power, and k_p and k_i are the proportional and integral gains of the PI controller, respectively.

C. Super capacitor Controller

The low-frequency model of a super capacitor consisting of a capacitor and a resistor, which can be used under power system operating frequency range, is employed in the current work. As shown in Fig. 1, the super capacitor is connected to the dc bus of the back-to-back converter using a bidirectional buck–boost converter system. The high-frequency component of the demand-generation mismatch P_{df} is met by the super capacitor where the corresponding reference current $(i_{sc})_{ref}$ is estimated using (20). The adopted control strategy for the super capacitor is illustrated in Fig. 15

$$(i_{sc})_{ref} = \frac{P_{hf}}{v_{sc}} \quad (20)$$

D. Dump Load Controller

Dump load is represented by a series of resistors that are connected across switches. The resistors are used

to operate at zero crossings of the voltage to ensure minimum impact on the quality of system voltage. As stated in Section III, the operation of dump load is enabled when the battery storage reaches its maximum capacity. Therefore, the condition under which the dump load operation is enabled is given by (21). It is to be noted that the contribution of the super capacitor power is not considered in the process of estimating the dump load power considering its performance in a short-term window and a high frequency domain. The simplified schematic of the dump load controller is shown in Fig. 16

$$P_d = \begin{cases} P_d, & (P_w) + (P_b)_{max} - P_L > 0 \\ 0, & \text{otherwise} \end{cases} \quad (21)$$

where P_w is the power output of the DFIG, and $(P_b)_{max}$ is the maximum capacity of the battery storage.

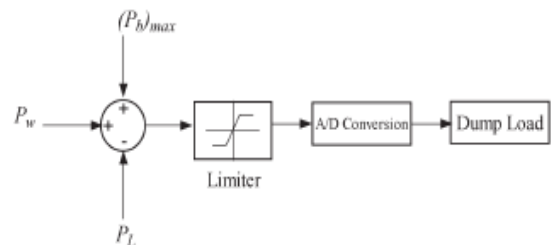


Fig.16. Dump load control strategy.

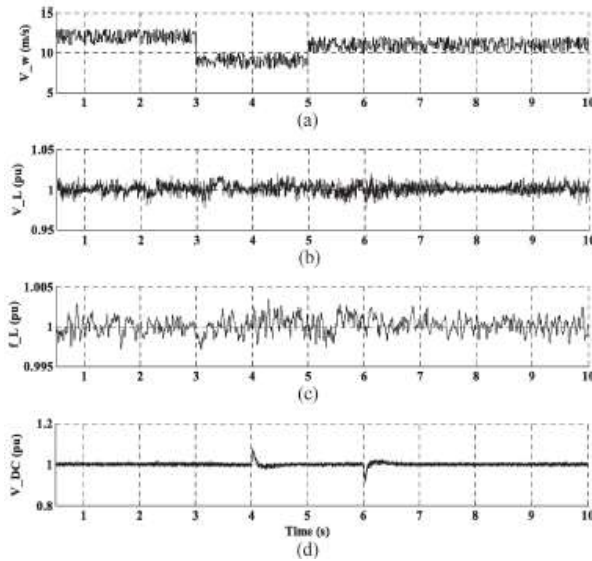


Fig. 17. Response of the DFIG-based RAPS system during variable wind and load conditions: (a) wind speed, (b) voltage on the load side, (c) frequency on the load side, and (d) dc link voltage.

VI. PERFORMANCE EVALUATION OF THE HYBRID ENERGY STORAGE IN A DFIG-BASED RAPS SYSTEM

The system response of the DFIG-based RAPS system is shown in Fig. 17. Fig. 18 illustrates the power sharing between different system components. The wind condition under which the system has been simulated is shown in Fig. 17(a). It is shown that the wind velocity is set initially at 12 m/s. At $t = 3$ s, the wind velocity drops to 9 m/s, and it increases to 11 m/s at $t = 5$ s. As shown in Fig. 18(d), initial load demand is set at 0.425 p.u., and then it is increased to a value of 0.7 p.u. at $t = 4$ s and the added additional load (i.e., 0.275 p.u.) is disconnected from the system at $t = 6$ s. The voltage on the load side is shown in Fig. 17(b), which is not seen to be affected by the wind speed or resistive load step changes. The load voltage of the system stays within $\pm 2\%$ of its rated value throughout the operation. The operating frequency of the RAPS system is shown in Fig. 17(c). As anticipated, the operating frequency is closely regulated at its rated value of 1.0 p.u. and is not seen to be influenced by the wind speed or load step changes. Furthermore, it can be seen that the

frequency of the system is maintained within $\pm 0.2\%$ of its rated value. The dc link voltage of the DFIG is depicted in Fig. 17(d), which is well regulated at its rated value throughout the operation except during load step changes. However, the highest dc link voltage variations are seen to occur at $t = 4$ s

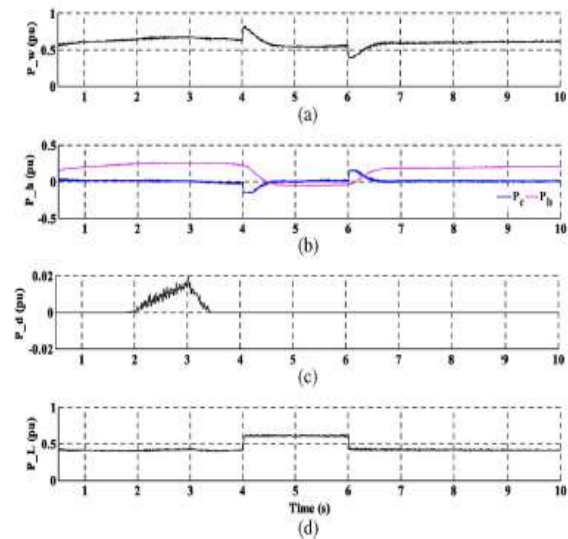


Fig. 18. Power sharing of the DFIG-based wind-hybrid energy storage RAPS system during variable wind and load conditions: (a) wind power, (b) hybrid energy storage power (i.e., battery power P_b and super capacitor power P_{sc}), (c) dump load power, and (d) load demand.

And $t = 6$ s, which correspond to the load step changes, as evident from Fig. 17(d). It can be noted that the super capacitor quickly changes its direction of power flow, as evident from Fig. 18(b), which causes the fluctuations in the dc link voltage. However, even during such transient conditions, the dc link voltage variation is limited to within $\pm 10\%$ of its rated value.

The DFIG power output is shown in Fig. 18(a). For simulation purposes, initially, the slip of the wind turbine is set to $s = -0.1$, which corresponds to super synchronous mode of operation. According to the wind turbine characteristics, the corresponding maximum power output of the wind generator is 0.73

p.u. at the speed of 1.2 p.u. for a wind speed of 11 m/s. As shown in Fig. 18(a), the power output of the DFIG is seen to rise to a value of 0.69 p.u. at $t = 3$ s, and the corresponding load demand is at 0.425 p.u. This situation simulates an over generation condition where the excess power is shared between the battery storage system and super capacitor, as evident from Fig. 18(b). It is shown that the super capacitor responds to the fast-varying power variations, whereas the battery absorbs the slow-varying power variations of the demand-generation mismatch. In addition, the super capacitor quickly responds to load step changes that occur at $t = 4$ s and $t = 6$ s avoiding high rates of DOD of the battery storage system. Furthermore, the battery storage system reaches its full capacity at $t = 2$ s leading to the operation of dump load, which absorbs the additional power, as evident from Fig. 18(c). The battery storage system operates in its charging mode until load step addition, which occurs at $t = 4$ s leading to a change of its mode of operation from charging to discharging. However, the rate of discharge is reduced after the load step reduction that occurs at $t = 6$ s. The MPPT behavior of the DFIG is shown in Fig. 19. It is shown that DFIG closely follows the MPPT curve except during the transient conditions that occur at $t = 4$ s and $t = 6$ s.

The battery current for the case with no super capacitor is shown in Fig. 20. The battery current consists of a high frequency fluctuating component, and it exhibits steep DOD

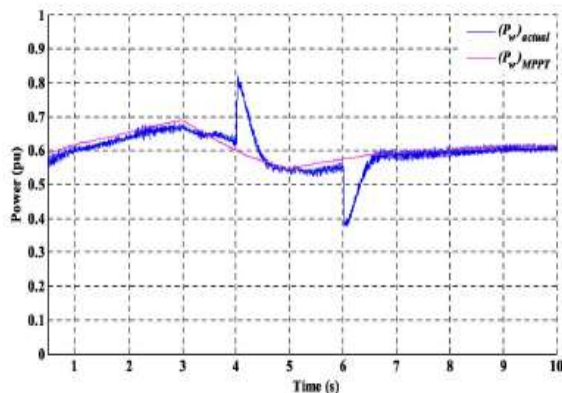


Fig.19. MPPT tracking capability of the DFIG in a RAPS system with energy storage integrated.

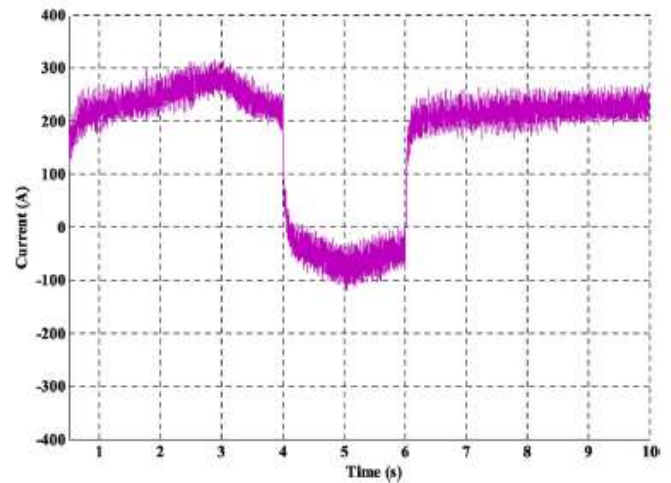


Fig. 20. Battery current for the case with no super capacitor of the DFIG based RAPS system with hybrid energy storage integrated.

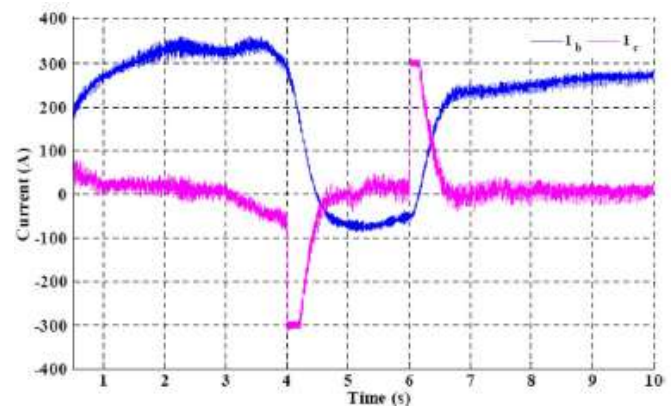


Fig. 21. Currents of the hybrid energy storage: battery current i_b and super capacitor current i_c of the DFIG-based RAPS system

During load step changes. The current levels of the hybrid energy storage with the super capacitor are shown in Fig. 21. It is shown that the battery storage system has less fluctuation in its current with low DOD rate at the time of load step changes compared with the case where it operates alone without a super capacitor.

The super capacitor current consists mostly of high-frequency component and is seen to quickly respond to the transients.

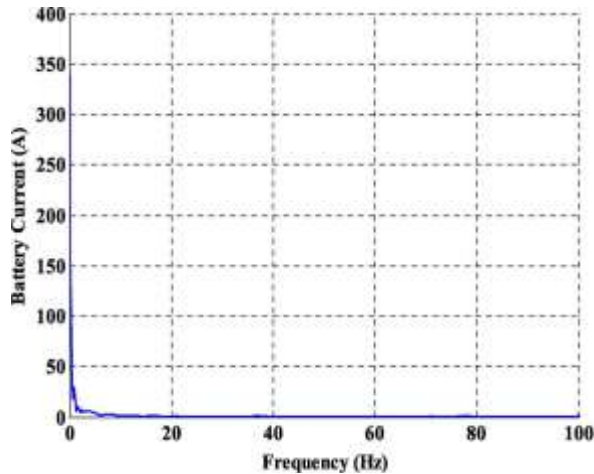


Fig. 22. Frequency spectrum of the battery storage system of hybrid energy storage.

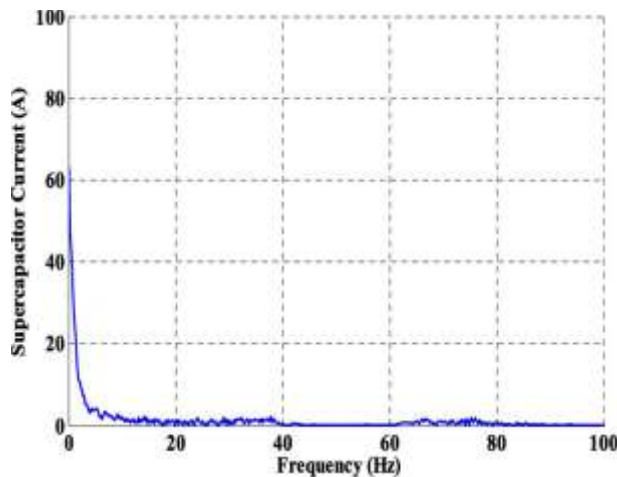


Fig. 23. Frequency spectrum of the super capacitor in hybrid energy.

However, the safety feature integrated with the controller of the super capacitor has limited its current to 300 A.12

The frequency spectra of the battery current and the super capacitor current are given in Figs. 22 and 23, respectively. The battery current is shown to be free from ripples or high-frequency component, whereas the super capacitor current consists of considerable amount of high frequencies, 13 which ensures the safe operation of the battery storage

VII. CONCLUSION

This paper has addressed the benefits of integrating a super- capacitor to a battery storage system in a wind-based hybrid RAPS system. In this regard, a power management algorithm has been established between the battery storage system and super capacitor to operate both energy storage systems in a designated manner. In addition, to coordinate the power flow between the RAPS system components, a control coordination strategy was developed and implemented by incorporating the

TABLE I

PARAMETERS ASSOCIATED WITH RAPS SYSTEM

Rated power output (P_{rated})	250 kW
Static resistance (R_s)	0.00709 m Ω
stator Leakage inductance (L_{ls})	0.171 mH
Rotor resistance (R_r)	0.005 m Ω
Rotor leakage inductance (L_{lr})	0.156 mH
Magnetising inductance (L_m)	2.2 Vs
Inertia constant (H)	2.04 s
Number of pole pairs (P)	2
Filter inductance at LSC (L_f)	0.2 mH
Filter resistance at LSC (R_f)	0.3 m Ω
DC bus voltage (V_{dc})	750 V
Stator voltage (V_s)	400 V
Operating frequency (f_e)	50 Hz
Rating of battery storage system (P_b)	120 kW
Capacitance of Supercapacitor (C)	20 F
Allowable SOC of the battery system (SOC)	40%–80%
Road dump load power (P_{load})	200 kW

Afore mentioned power management algorithm. Furthermore, the following conclusions can be drawn.

- 1) The proposed RAPS system is able to regulate the voltage and frequency on the ac side within tight limits.
- 2) The algorithm to satisfy demand-generation mismatch has been implemented using the proposed power management algorithm where the demand-generation mismatch of the RAPS systems was split in the two frequency operating regions using a high-pass filter. The high- frequency power component

was managed through the super capacitor while leaving the low-frequency power component for the battery storage system.

3) The maximum power extraction through the DFIG has been achieved by coordinating the operation of hybrid energy storage system by implementing the maximum power extraction algorithm.

4) The reduction of the rate of DODs has been achieved by operating the super capacitor to respond the high- frequency power component associated with the demand- generation mismatch, thus avoiding high rate of DOD on the battery energy storage system.

APPENDIX A

The parameters associated with the RAPS system are shown in Table I.

APPENDIX B

BATTERY INVERTER CONTROL FOR DFIG-BASED RAPS SYSTEM

The control algorithm associated with the inner current control loop of the battery inverter system given in Section V-B can be described as follows:

$$v_{ds1} = v_{ds} - v_{ds}^* + L_f \omega i_{qs} \quad (B.1)$$

$$v_{qs1} = v_{qs} - v_{qs}^* - L_f \omega i_{ds} \quad (B.2)$$

$$v_{ds}^* = R_f i_{ds} + L_f \frac{di_{ds}}{dt} \quad (B.3)$$

$$v_{qs}^* = R_f i_{qs} + L_f \frac{di_{qs}}{dt} \quad (B.4)$$

where v_a , v_b , and v_c are the voltages on the load side; i_a , i_b , and i_c are the currents through the filter circuit; L_f and R_f are filter inductance and resistance, respectively; v_{d1} , v_{q1} , and v_{c1} are the voltages at the inverter output; v_{ds} and v_{qs} are the d- and q-axis components of the load-side ac voltage, respectively; i_{ds} and i_{qs} are the d- and q-axis components of the inverter current, respectively; and v_{d1} and v_{q1} are

the d- and q-axis components of the inverter output voltage, respectively.

The d- and q-axis reference currents of the battery inverter can be generated by defining the reference active and reactive power components, as given in (B.5) and (B.6), respectively,

$$(i_{ds})_{ref} = ((P_b)_{ref} - P_b) (K_{pdb} + K_{idb}/s) \quad (B.5)$$

$$(i_{qs})_{ref} = ((Q_b)_{ref} - Q_b) (K_{pqb} + K_{iqb}/s) \quad (B.6)$$

where $(P_b)_{ref}$ and $(Q_b)_{ref}$ are the reference active and reactive power outputs of the battery inverter, and K_{pdb} , K_{pqb} and K_{idb} , K_{iqb} are the proportional and integral gains of the battery inverter controller.

APPENDIX C

ESTIMATION OF SUPERCAPACITOR SIZE

The super capacitor is used to supply s_{max} times the rated capacity of the DFIG power, i.e., P_{DFIG} . The safe operating voltage limits associated with the super capacitor are selected to be as follows:

$$250 \text{ V} < v_{sc} < 500 \text{ V}. \quad (C.1)$$

Assuming that, in the worst case scenario, the super capacitor is able to provide the maximum slip power of DFIG $s_{max} P_{DFIG}$ for time $t = 10 \text{ s}$, the capacitance value of the super capacitor can be calculated as follows:

$$C = \frac{s_{max} (P_{DFIG})_{rated} t}{((v_{sc})_{max})^2 - ((v_{sc})_{min})^2} \quad (C.2)$$

$$C = \frac{0.3 \times 750 \times 1000 \times 10 \times 2}{500^2 - 200^2} \approx 20 \text{ F}. \quad (C.3)$$

REFERENCE

[1] M.-S. Lu, C.-L. Chang, W.-J. Lee, and L. Wang, "Combining the wind power generation system with energy storage equipment," IEEE Trans. Ind. Appl., vol. 45, no. 6, pp. 2019–2115, Nov./Dec. 2009.

- [2] Q. Li, S. S. Choi, Y. Yuan, and D. L. Yao, "On the determination of battery energy storage capacity and short-term power dispatch of a wind farm," *IEEE Trans. Sustainable Energy*, vol. 2, no. 2, pp. 148–158, Apr. 2011.
- [3] P. F. Ribeiro, B. K. Johnson, M. L. Crow, A. Arsoy, and Y. Liu, "Energy storage systems for advanced power applications," *Proc. IEEE*, vol. 89, no. 12, pp. 1744–1756, Dec. 2001.
- [4] M. Beaudin, H. Zareipour, A. Schellenberglobe, and W. Rosehart, "Energy storage for mitigating the variability of renewable electricity sources: An updated review," *Energy Sustainable Develop.*, vol. 14, no. 4, pp. 302–314, Dec. 2010.
- [5] T. Patrick and Moseley, "Energy storage in remote area power supply (RAPS) systems," *J. Power Sources*, vol. 155, no. 1, pp. 83–87, Apr. 2006.
- [6] W. Li, G. Joos, and J. Belanger, "Real-time simulation of a wind turbine generator coupled with a battery super capacitor energy storage system," *IEEE Trans. Ind. Electron.*, vol. 57, no. 4, pp. 1137–1145, Apr. 2010.
- [7] P. Thounthong, S. Rael, and B. Davat, "Control strategy of fuel cell and super capacitors association for a distributed generation system," *IEEE Trans. Ind. Electron.*, vol. 54, no. 6, pp. 3225–3233, Dec. 2007.
- [8] L. Qu and W. Qiao, "Constant power control of DFIG wind turbines with super capacitor energy storage," *IEEE Trans. Ind. Appl.*, vol. 47, no. 1, pp. 359–367, Jan./Feb. 2011.
- [9] S. Teleke, M. E. Baran, A. Q. Huang, S. Bhattacharya, and L. Anderson, "Control strategies for battery energy storage for wind farm dispatching," *IEEE Trans. Energy Convers.*, vol. 24, no. 3, pp. 725–732, Sep. 2009.
- [10] A. Abedini and H. Nikkhajoei, "Dynamic model and control of a wind- turbine generator with energy storage," *IET Renew. Power Gen.*, vol. 5, no. 1, pp. 67–78, Jan. 2011.
- [11] W. Li and G. Joos, "Dynamic model and control of a wind-turbine generator with energy storage," in *IEEE PESC*, Rhodes, Greece, Jun. 2008, pp. 1762–1768.
- [12] N. Mendis, K. Muttaqi, and S. Perera, "Voltage quality behavior of a wind turbine based remote area power system," in *Proc. IEEE ICIT*, Gippsland, Australia, Feb. 10–13, 2008, pp. 1–6.
- [13] S. T. Tentzerakis and S. A. Papathanassiou, "The harmonics of the slip energy recovery drive," *IEEE Power Eng. Rev.*, vol. 21, no. 4, pp. 55–57, Apr. 10–13, 2001.
- [14] L. Hamefors and H. P. Nee, "Model-based current control of AC machines using the internal model control method," *IEEE Trans. Ind. Appl.*, vol. 34, no. 1, pp. 133–141, Jan./Feb. 1998.
- [15] J. C. Basilio and S. R. Matos, "Design of PI and PID controllers with transient performance specification," *IEEE Trans. Educ.*, vol. 45, no. 4, pp. 364–370, Nov. 2002.
- 16][Online]. available: <http://www.maxwell.com/products>



J. Srinu Naick received his B.E degree in Electrical & Electronics Engineering from Andhra University Vishakhapatnam AP,

India in 2003 and M.Tech with Energetics from NIT Calicut, Calicut, and Kerala, India in 2007. He is having 13 years of teaching and research experience. He is currently Associate Professor & Head in the Department of Electrical & Electronics Engineering, STNVR Engineering college, Jonnalagadda, Narasaraopet, Guntur, AP, India. His Research interests are in the areas of Power systems Industrial Drives & FACTS Controllers.

Email id: speaksrinu@gmail.com



Mr. Arepalli Narasimha Murthy M.Tech (Power and Industrial Drives Engineering) Pursuing In Sai Tirumala Nvr Engineering College

EMail id: mdnarasimha203@gmail.com